Bioconjugate Chemistry

pubs.acs.org/bc

Article

Characterization of Intrinsically Radiolabeled Poly(lactic-*co*-glycolic acid) Nanoparticles for ex Vivo Autologous Cell Labeling and in Vivo Tracking

Massis Krekorian,* Gerwin G. W. Sandker, Kimberley R. G. Cortenbach, Oya Tagit, N. Koen van Riessen, René Raavé, Mangala Srinivas, Carl G. Figdor, Sandra Heskamp, and Erik H. J. G. Aarntzen

Cite This: *Bioconjugate Chem.* 2021, 32, 1802−1811

Read Online

ACCESS | Metrics & More | Article Recommendations | Supporting Information

ABSTRACT: With the advent of novel immunotherapies, interest in ex vivo autologous cell labeling for in vivo cell tracking has revived. However, current clinically available labeling strategies have several drawbacks, such as release of radiolabel over time and cytotoxicity. Poly(lactic-*co*-glycolic acid) nanoparticles (PLGA NPs) are clinically used biodegradable carriers of contrast agents, with high loading capacity for multimodal imaging agents. Here we show the development of PLGA-based NPs for ex vivo cell labeling and in vivo cell tracking with SPECT. We used primary amine-modified PLGA polymers (PLGA-NH_2) to construct NPs similar to unmodified PLGA NPs. PLGA-NH_2 NPs were efficiently radiolabeled without chelator and retained the radionuclide for 2 weeks. Monocyte-derived dendritic cells labeled with [^{111}In]In-PLGA-NH_2 showed higher specific activity than those labeled with [^{111}In]In-oxine, with no negative effect on cell viability. SPECT/CT imaging showed that radiolabeled THP-1 cells accumulated at the *Staphylococcus aureus* infection site in mice. In conclusion, PLGA-NH_2 NPs are able to retain ^{111}In, independent of chelator presence. Furthermore, [^{111}In]In-PLGA-NH_2 allows cell labeling with high specific activity and no loss of activity over prolonged time intervals. Finally, in vivo tracking of ex vivo labeled THP-1 cells was demonstrated in an infection model using SPECT/CT imaging.

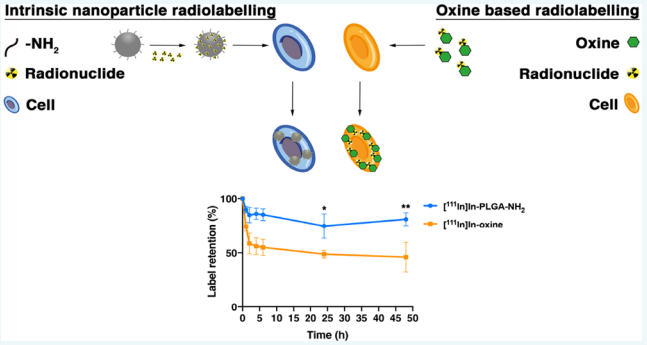

INTRODUCTION

Cell-based immunotherapy is a potentially effective cancer treatment, but unresolved issues hamper its broad implementation. For example, severe side effects due to unwanted relocalization of therapeutic cells in vivo, or limited efficacy when tumor tissues are not reached. In vivo imaging of ex vivo labeled cells offers a potential tool to study these questions. This technique would enable clinicians to distinguish responders from nonresponders early during treatment, reducing costs and avoiding adverse events.[1,2] Current clinically available cell tracking methods rely on using lipophilic agents (oxine and hexamethylpropyleneamine oxime (HMPAO)), which are gradually released from cells, resulting in limited specific activity.[3−5] Here nanoparticles (NPs), which generally show minimal efflux and have a high capacity to bind radiometals, might have a role.

Poly(lactic-*co*-glycolic acid) polymers (PLGA) are widely used for NP synthesis. Their favorable biodegradation characteristics (fast clearance and low toxicity) combined with their encapsulation capabilities make PLGA NPs ideal carriers for in vivo delivery of drugs and contrast agents.[6,7] Due to the hydrophobic core, PLGA NPs are able to encapsulate hydrophobic compounds, including, for example, dyes for fluorescent imaging (FI) and metals for magnetic resonance imaging (MRI).[8,9] Furthermore, recent findings suggest additional intrinsic ultrasound characteristics of the NPs without the need for contrast agents.[10] These characteristics make the NPs highly suitable for multimodal in vivo cell tracking.[11]

In contrast to MRI, FI and ultrasound, single-photon emission computed tomography (SPECT) and positron emission tomography (PET) have higher sensitivity and enable whole-body imaging, which is required for in vivo immune cell tracking.[12] For this purpose, radiolabeling of PLGA NPs need to be efficient (for detection of small number of cells) and

Received: May 23, 2021
Revised: June 11, 2021
Published: June 23, 2021

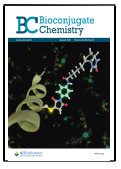

https://doi.org/10.1021/acs.bioconjchem.1c00271
Bioconjugate Chem. 2021, 32, 1802−1811

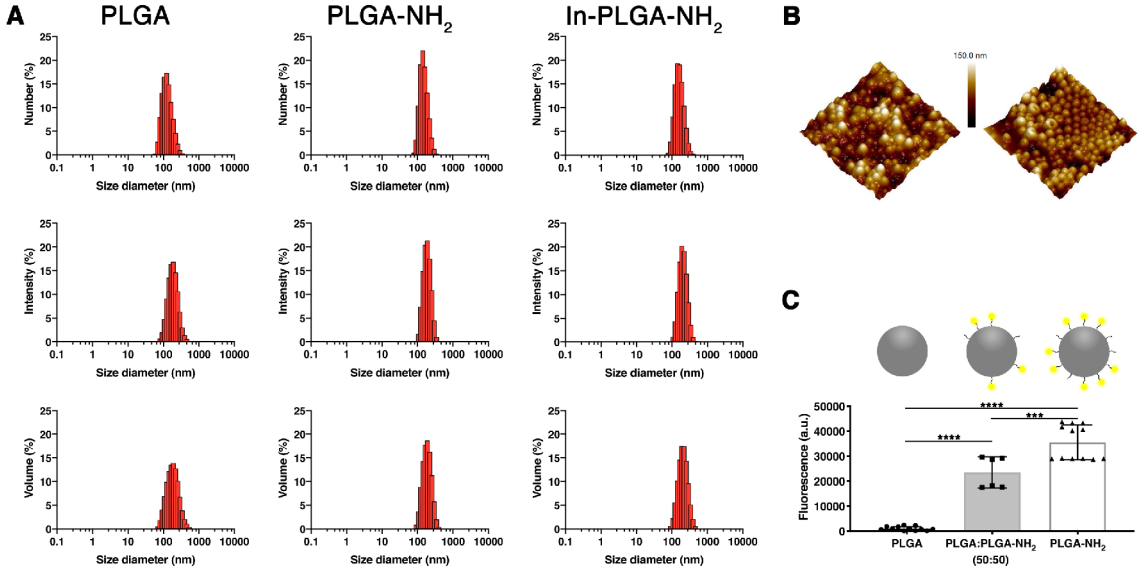

Figure 1. Characteristics of PLGA, PLGA-$NH_2$and In-PLGA-NH_2NPs. (A) Diameter of PLGA, PLGA-NH_2, and In-PLGA-NH_2 NPs as measured with dynamic light scattering. (B) Atomic force microscopy of the same particles. Scale: from corner to corner represents 2 μm. (C) Fluorescamine conjugation to PLGA (n = 12), PLGA:PLGA-NH_2 (50:50, n = 6) and PLGA-NH_2 NPs (n = 12). ***P = 0.0002, ****P < 0.0001.

stable over time (to prevent nonspecific accumulation in other cells). Intrinsic labeling, e.g. without additional chelator, of the particles is preferred, to avoid additional radiochemical procedures and particle modifications.

The aim of this study was to develop PLGA-based NPs that allow ex vivo ^{111}In-labeling of cells for in vivo cell tracking using SPECT/CT. Here we report the in vitro NP stability, intrinsic radiolabeling efficiency, and label retention under various conditions. Furthermore, we present the in vivo [^{111}In]In-PLGA-NH_2 NP stability, blood clearance, and biodistribution in mice, as measured by ex vivo biodistribution studies and SPECT/CT imaging. Also, we compared ex vivo cell labeling efficiency, viability, and retention of [^{111}In]In-PLGA-NH_2 NPs with [^{111}In]In-oxine over an extended period. Finally, we show in vivo accumulation of ex vivo labeled [^{111}In]In-THP-1 cells in a *Staphylococcus aureus* (*S. aureus*) infection model.

RESULTS

Particle Synthesis and Characterization. PLGA-NH_2 NPs were prepared as described previously,[8] using polymers with a primary amine linker. Diameter, polydispersity index (PDI), and zeta potential did not differ between the two NP formulations (Figure 1 and Table 1).

Accessibility of the primary amines was necessary to couple the chelator DTPA to the NPs we tested this using fluorescamine.[13] Three compositions of particles were used: 100% PLGA, a 50:50 ratio of PLGA:PLGA-NH_2, and 100% PLGA-NH_2 (Figure 1C). PLGA NPs that contain no primary amine groups produced a low fluorescent signal (mean of 1070 ± 779 arbitrary units (a.u.)), while mean fluorescent intensities of 23 475 ± 6241 au and 35 544 ± 6953 au were observed for PLGA:PLGA-NH_2 (50:50, p < 0.0001) and PLGA-NH_2 NPs (p < 0.0001), respectively. This indicated that the PLGA-NH_2 polymers retain the amine groups which were still accessible for coupling to fluorescamine. The structure of the PLGA and PLGA-NH_2 particles was stable for 24 h both in PBS and in 100% human serum (Figure S1).

Table 1. Characterization of PLGA, PLGA-NH_2, and In-PLGA-NH_2 NPs: Size (n = 3), PDI (n = 3), and Zeta Potential (n = 3)

sample	diameter (nm)	polydispersity (PDI)	zeta potential (mV)
PLGA	184 ± 18	0.10	−2.9 ± 0.85
PLGA-NH_2	182 ± 11	0.06	−2.2 ± 0.31
In-PLGA-NH_2	194 ± 1	0.09	−2.5 ± 0.67

^{111}In-Labeling and in Vivo Distribution of Particles. Radiolabeling of ITC-DTPA conjugated and nonconjugated PLGA and PLGA-NH_2 NPs was performed with [^{111}In]$InCl_3$. ^{111}In-labeling of PLGA-NH_2 NPs was efficient with and without DTPA (DTPA-PLGA-NH_2 and PLGA-NH_2, respectively) as a chelator (Figure 2B). The labeling efficiency was 42 ± 4% for DTPA-PLGA-NH_2 compared with 87 ± 1% for PLGA-NH_2 NPs (p < 0.0001), while the unmodified PLGA NPs had a labeling efficiency of <1% for both DTPA conjugated and nonconjugated (p = 0.9992).

Next, we compared labeling efficiency in different buffers. NH_4Ac buffer showed the highest labeling efficiency of 81 ± 10% compared with 71 ± 1% for MES (ns) and 53 ± 7% (p = 0.002) for HEPES for PLGA-NH_2 NPs (Figure 2C). For all buffers, DTPA-PLGA-NH_2 NPs were labeled with lower efficiency compared with PLGA-NH_2NPs. On the basis of these results, NH_4Ac was used in subsequent experiments. In vitro stability studies in PBS and 100% human serum (Figure S2) showed that ^{111}In was not released from the PLGA-NH_2 NPs over a period of 2 weeks. Furthermore, minimal release of the ^{111}In was observed when the particles were challenged with EDTA.

The kinetics of the labeled NPs were studied in vivo, showing that [^{111}In]In-PLGA-NH_2 NPs were rapidly cleared from the circulation and accumulated in spleen, liver, lymph nodes, and bone marrow (Figure S3 and Table S1). The blood half-life was 58 ± 15 min. Overall, the observed clearance and organ biodistribution of [^{111}In]In-PLGA-NH_2 NPs was in accordance with previous PLGA NP biodistributions,[14] with

https://doi.org/10.1021/acs.bioconjchem.1c00271
Bioconjugate Chem. 2021, 32, 1802−1811

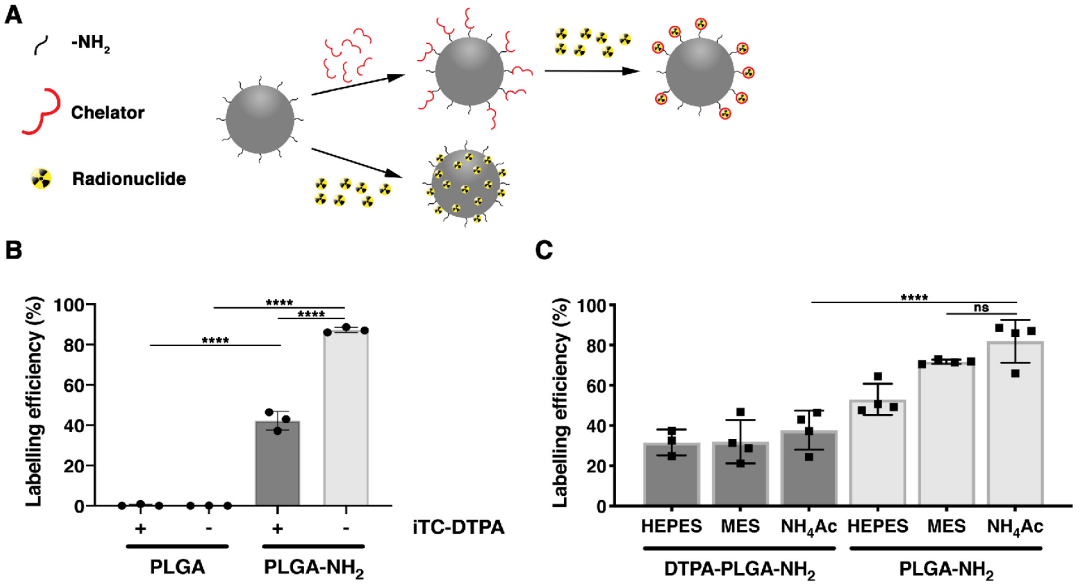

Figure 2. ^{111}In-labeling of nanoparticles. (A) Cartoon of proposed mechanisms for radiolabeling of PLGA-NH_2 NP with and without a chelator. (B) Specific labeling of PLGA and PLGA-NH_2 with [^{111}In]$InCl_3$ with and without conjugation of DTPA (n = 3). (C) DTPA conjugated and nonconjugated PLGA-NH_2 NPs for ^{111}In-labeling in 0.5 M and pH 5.5 HEPES, MES, and NH_4Ac labeling buffers (n = 3−4). ns = not significant, ****P < 0.0001.

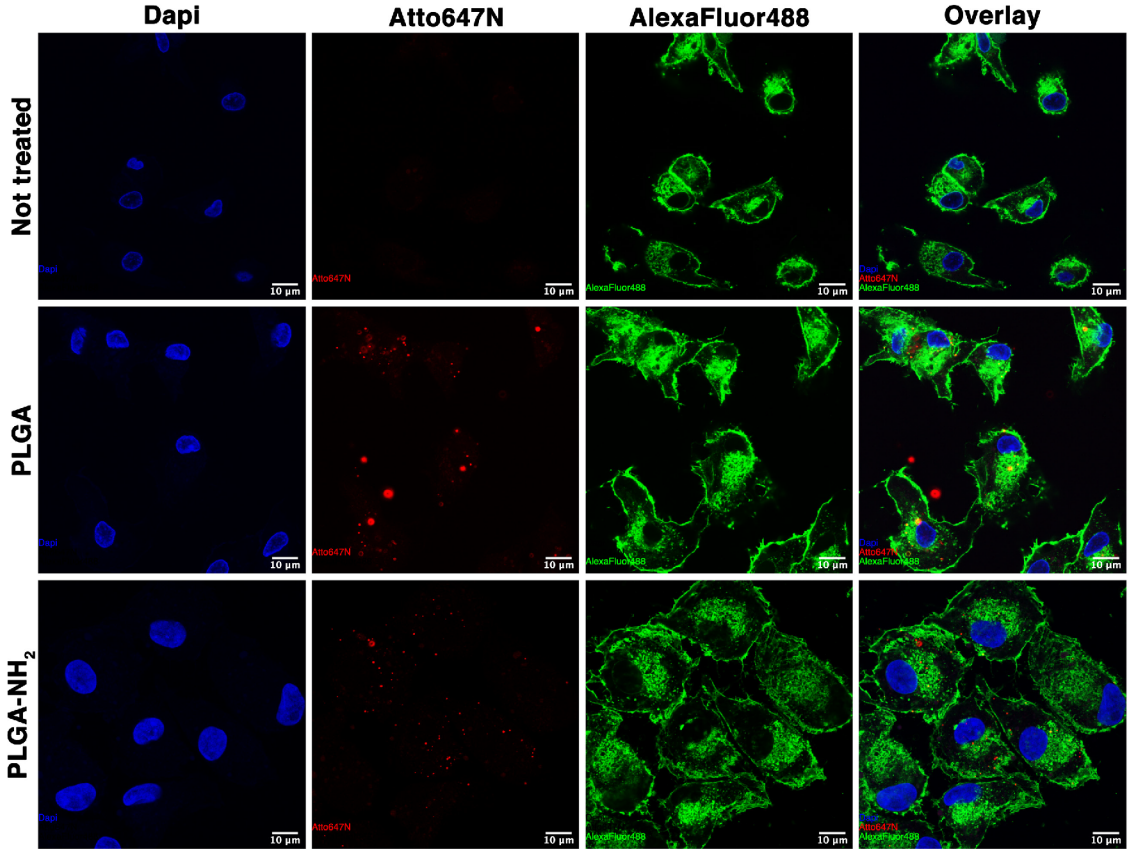

Figure 3. Confocal imaging of monocyte-derived dendritic cells after labeling with PLGA and PLGA-NH_2NPs. Monocyte-derived dendritic cells (moDC) labeled without NPs, with atto647N dye encapsulated PLGA, or with PLGA-NH_2 NPs for 2 h at culture conditions. The cells were stained for the nucleus with dapi (blue) and cell membrane with AlexaFluor488-conjugated wheat germ agglutinin (green). The atto647N dye (red)-encapsulating NPs are indicated in red. For optimal visualization of the atto647N dye, the brightness was increased for the red channel in all samples with similar settings in Fiji. Scale bar = 10 μm.

rapid blood clearance and high accumulation in spleen and liver.

Confocal Imaging of atto647N Dye-Encapsulated PLGA-NH_2 NPs in Monocyte-Derived Dendritic Cells.

https://doi.org/10.1021/acs.bioconjchem.1c00271
Bioconjugate Chem. 2021, 32, 1802−1811

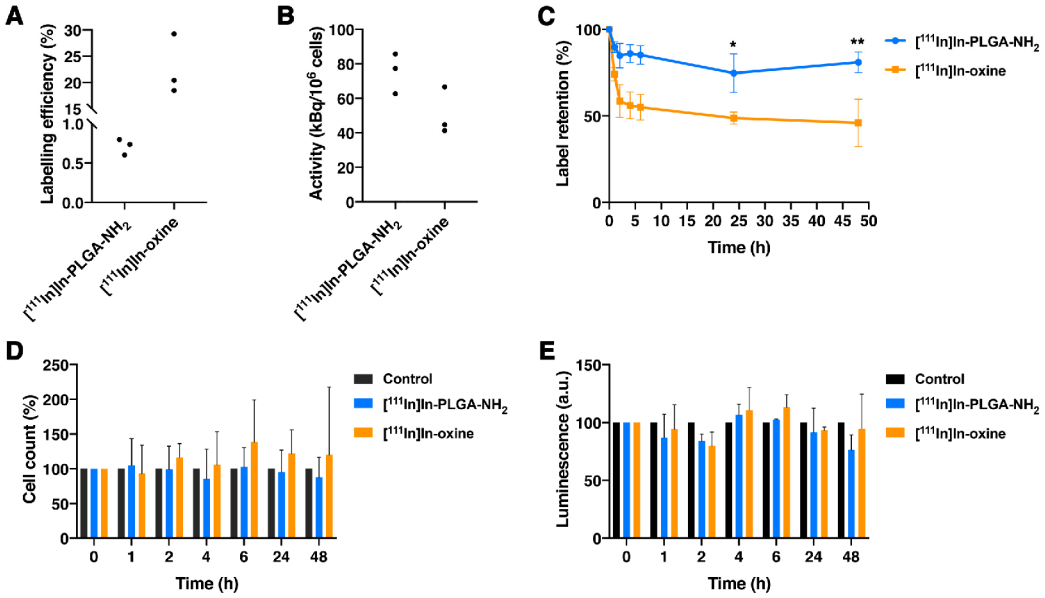

Figure 4. Monocyte-derived dendritic cell (moDC) labeling and retention of radionuclide over time. (A) Labeling efficiency of [^{111}In]In-PLGA-NH_2 and [^{111}In]In-oxine-labeled moDC cells after 1 h and 15−20 min incubation at culture conditions, respectively (n = 3). (B) Specific activity in kBq per 1 × 10^6 cells, measured on the cell pellet after three washing steps (n = 3). (C) The radioactivity on the cells was measured before and after incubation at culture conditions for 1, 2, 4, 6, 24, and 48 h (n = 5−6). (D) Cell numbers were counted with trypan blue staining after the label retention (n = 5−6). (E) After counting the cells, the viability was measured with the CellTiter-Glo assay (n = 5−6). In all experiments, controls were moDC cells treated similar to other conditions without the addition of [^{111}In]In-PLGA-NH_2or [^{111}In]In-oxine. *P = 0.0110, **P = 0.0052.

To determine whether PLGA and PLGA-NH_2 NPs are internalized by cells or only sticking to the cell membrane, we incubated monocyte-derived dendritic cells (moDC) with atto647N dye-encapsulating PLGA and PLGA-NH_2 NPs for confocal imaging. Figure 3 shows an atto647N signal in cells incubated with PLGA and PLGA-NH_2 NPs. A z-stack is available as videos S1−S3.

MoDC Labeling with [^{111}In]In-PLGA-NH_2 NPs and Retention over Time. The cell labeling potential of [^{111}In]In-PLGA-NH_2 NPs was compared to that of [^{111}In]In-oxine using moDCs, isolated and differentiated from healthy donors. The amount of [^{111}In]In-PLGA-NH_2 taken up by the moDC cells (labeling efficiency) was 0.7 ± 0.1% compared to 22.7 ± 5.7% for [^{111}In]In-oxine (Figure 4A), resulting in a specific activity of 75 ± 12 kBq/10^6 cells and 51 ± 14 kBq/10^6 cells, respectively (Figure 4B). Retention of the radiolabel after 48 h incubation at culture conditions was 80.9 ± 6.0% for [^{111}In]In-PLGA-NH_2, which was significantly higher compared with 46.0 ± 13.7% for [^{111}In]In-oxine (p = 0.0052, Figure 4C). Furthermore, incubation of the cells at culture conditions for 48 h did not have a significant effect on the number of cells and ATP content (Figure 4, parts D and E, respectively).

In Vivo SPECT/CT Imaging of [^{111}In]In-PLGA-NH_2 NP Labeled THP-1 Cells. To study the detection sensitivity of [^{111}In]In-PLGA-NH_2 NPs for in vivo cell tracking, [^{111}In]In-PLGA-NH_2 NPs alone in Matrigel, and 10 000 or 100 000 [^{111}In]In-PLGA-NH_2 NP-labeled THP-1 cells in Matrigel, were injected subcutaneously. All conditions, including the lowest number of 10 000 [^{111}In]In-PLGA-NH_2 NP-labeled THP-1 cells, were clearly visible using SPECT/CT (Figure 5). Biodistribution studies showed comparable and low radioactivity levels in bone marrow and blood for all conditions, indicating that there was minimal loss of radioactivity from NPs or radiolabeled THP-1 cells in Matrigel over 24 h (Figure S4 and Table S2).

Tracking of [^{111}In]In-THP-1 Cells to Local *S. aureus* Infection BALB/CAnN.Cg-Foxn1nu/Crl Mice Model. As a next step, a model of local intramuscular *S. aureus* infection was used for in vivo tracking of the ex vivo labeled [^{111}In]In-THP-1 cells. Intramuscular injection with PBS/blood mixture in the contralateral hind leg served as control. An increase in activity at the site of local infection was visible with SPECT/CT over 24 h (Figure 6). In vivo distribution was as expected with rapid clearance of the THP-1 cells from blood and accumulation in the lung, liver, spleen, and bone marrow (Figure S5 and Table S3). Ex vivo biodistribution studies demonstrated that 0.69 ± 0.23% (corresponding to 34 499 ± 11 276 cells) of the radiolabeled THP-1 cells accumulated in the *S. aureus* infected muscles, compared to 0.02 ± 0.02% (1089 ± 791 cells) for the control muscle. The number of cells calculated was in line with the Matrigel study, indicating that it was possible to track a low number of THP-1 cells labeled with [^{111}In]In-PLGA-NH_2 NPs.

DISCUSSION

In vivo tracking of small numbers of cells requires highly sensitive imaging modalities and sufficient radiolabel retention over a prolonged period of time. Current passive membrane diffusion methods for ex vivo immune cell labeling are insufficient in this respect due to efflux of the radiolabel from the cells. To address this, we developed an ^{111}In-labeled GMP-compatible PLGA-NH_2-based nanoparticle for SPECT imaging.

The newly developed PLGA-NH_2 NPs have a small primary amine (NH_2) linker on the surface, which allows for intrinsic radiolabeling. Synthesis of the NPs did not affect the availability of the amine linkers on the surface, which was also shown by Wongrakpanich et al.[15] PLGA-NH_2 NPs remained stable in PBS for up to 2 weeks while in human serum their size increased to >200 nm. Under in vivo

https://doi.org/10.1021/acs.bioconjchem.1c00271
Bioconjugate Chem. 2021, 32, 1802−1811

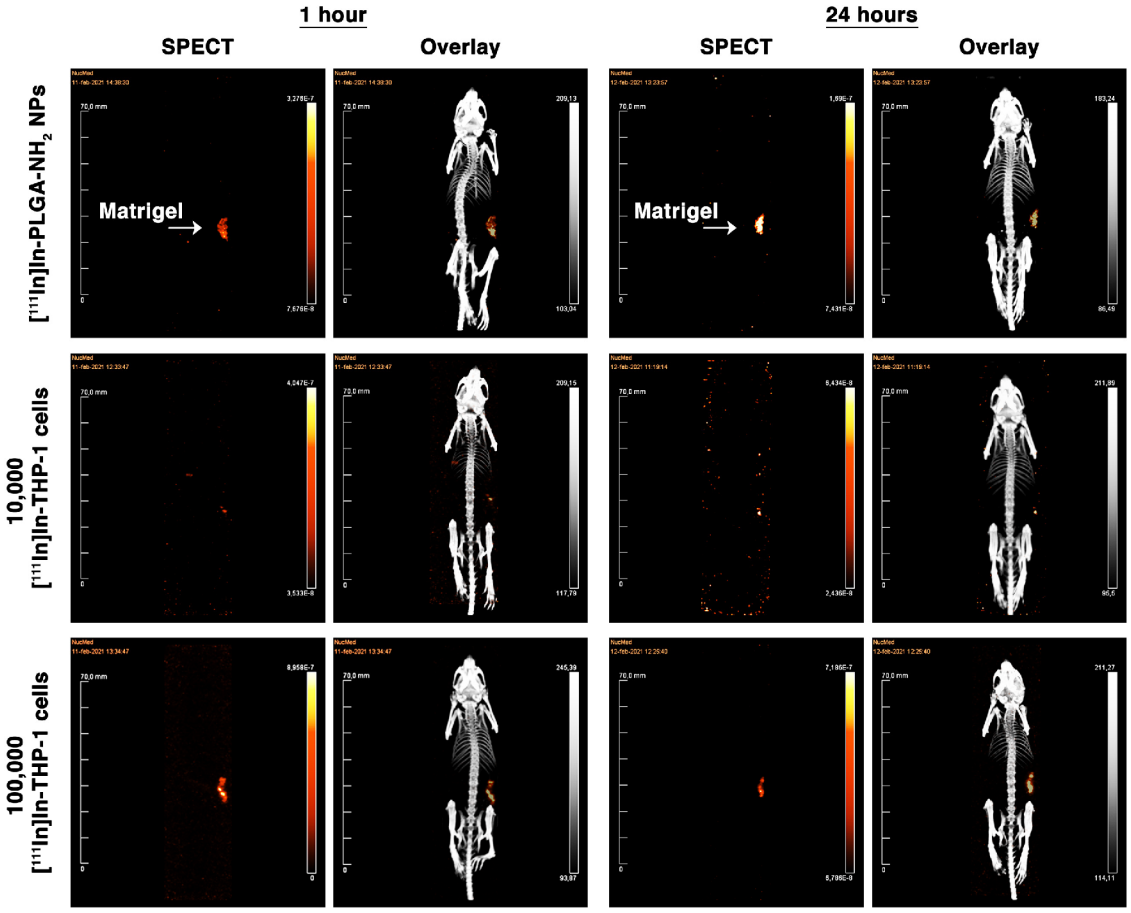

Figure 5. In vivo SPECT/CT images of ex vivo [^{111}In]In-PLGA-NH_2-labeled THP-1 cells in Matrigel. After ex vivo labeling of the THP-1 cells, the cells were mixed with Matrigel and subcutaneously injected in BALB/cAnNRj-Foxn1nu/Foxn1nu mice. Mice were injected with either [^{111}In]In-PLGA-NH_2 NPs (control), 10 000 [^{111}In]In-THP-1 cells, or 100 000 [^{111}In]In-THP-1 cells. Brightness (+68 points) and contrast (+47 points) of all the images were increased with Adobe photoshop for better visualization..

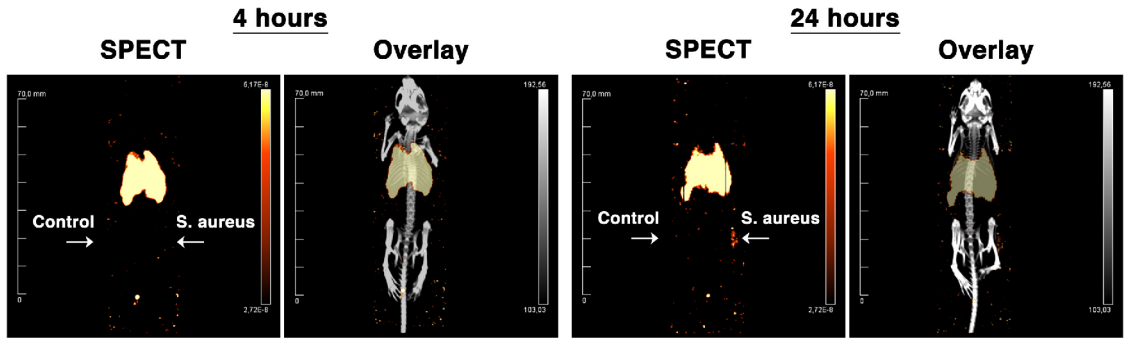

Figure 6. [^{111}In]In-THP-1 cell tracking in *Staphylococcus aureus* (*S. aureus*) model with SPECT/CT. BALB/CAnN.Cg-Foxn1nu mice were injected intramuscular in the right hind leg with *S. aureus*+blood and with PBS+blood (as a control) in the left hind leg before intravenous injection of ex vivo ^{111}In-labeled THP-1 cells ([^{111}In]In-THP-1, 5 × 10^6 cells/mouse). The [^{111}In]In-THP-1 cells were followed with SPECT/CT for 24 h.

conditions, this is known as corona formation and is attributed to the opsonization (coating with proteins) by serum proteins.[16−19] Because the ultimate purpose of these particles is to label cells ex vivo and the expected time to take up the particles by the cells is between 1 and 4 h, "corona formation" will be of limited influence on particle uptake. Interestingly, it was previously shown that the uptake of NPs by macrophages was increased in the presence of fetal calf serum (FCS),[20] most likely due to the recognition of proteins on the particle surface by cell receptors, resulting in enhanced phagocytosis.

PLGA-NH_2 NPs were efficiently and stably radiolabeled without using ITC-DTPA as chelator, but the exact radiolabeling mechanism is yet unknown. However, the structure of the linker could give us an indication, as it is similar to ethylenediamine, a small molecule with two nitrogen atoms on both ends that can act as chelator. Due to linkage to the polymer, it has lost one nitrogen atom,[21] but this can be compensated by the multipolymer structure of the NPs which provide a multitude of nitrogen atoms and together have the potential to chelate ^{111}In. The polymer conjugation with DTPA might disrupt the large surface area of the particles and

https://doi.org/10.1021/acs.bioconjchem.1c00271
Bioconjugate Chem. 2021, 32, 1802−1811

therefore reduce labeling efficiency with ^{111}In. In the literature, silica-based NPs have been shown to have similar characteristics where intrinsic labeling is facilitated by the mesoporous properties that enable the radionuclide to diffuse into and become trapped in the core of the NP.[22] Further studies are needed to unravel the exact mechanism of how the PLGA-NH_2 NP chelates ^{111}In. Radiolabeling was most efficient using NH_4Ac buffer, compared with HEPES and MES. The latter two have metal ion binding capacity (although at very low levels), which could explain their lower labeling efficiency.[23,24]

To study the in vivo distribution of the particles, we injected [^{111}In]In-PLGA-NH_2 NPs intravenously in immunocompetent mice, followed by blood sampling, SPECT/CT imaging, and ex vivo biodistribution studies. The blood half-life was 58 min, which is slower than other PLGA NPs (13−35 s for 63−750 μg polymer) but faster than PEGylated PLGA NPs (7 h).[25] As Qie et al. have shown, this could be attributed to the opsonisation of the particles, resulting in uptake by phagocytic cells from the mononuclear phagocyte system (MPS), which reside in the liver, spleen, lymph nodes, and bone marrow.[26−31]

[^{111}In]In-PLGA-NH_2 NPs were used to label a phagocytic cell type used for cell-based therapy and an established cell type for particle labeling:[11,32] moDC cells from healthy donors and results were compared to [^{111}In]In-oxine cell labeling. Cell labeling with [^{111}In]In-oxine is fast and with rather high loading efficiency. However, toxicity of oxine and leakage of the radionuclide from the cell are major drawbacks, as they can result in a high background signal during imaging.[33−35] Here we have shown that although the NP labeling efficiency is lower, we could achieve similar specific activity per cell and improved radiolabel retention. Radiolabeling of PLGA NPs and other NP platforms have been previously studied for different applications, from in vivo tracking of the NPs to targeting of immune cells for therapeutic purposes.[36−41] For example, Sirianni et al. used fluorine-18-labeled biotin coupled to avidin-PLGA NPs to measure NP delivery in rat brain with PET.[41] In another preclinical study, [^{89}Zr]Zr-DFO-dextran NPs were used for in vivo macrophage imaging in xenograft models.[42] Furthermore, a smart drug delivery system [^{177}Lu]Lu-DOTA-HA-PLGA(MTX) NPs for specific targeting of macrophages was evaluated in a rheumatoid arthritis model.[43] These modifications for specific targeting could also be applied for improved uptake of the nanoparticles for ex vivo cell labeling.

In vivo cell tracking has been performed previously, using different combinations of labeling methods and imaging modalities.[44−48] Here we used the human monocyte cell line THP-1, an intermediate phagocytic cell line. Monocyte cells are progenitor cells of macrophages, which respond to inflammation signals. Static in vivo imaging showed that subcutaneous deposits of 10 000 and 100 000 radiolabeled cells were visible at 1 and 24 h post cell transplantation, demonstrating the feasibility to image low numbers of cells. In a subsequent proof-of-concept study, [^{111}In]In-THP-1 cells were injected intravenously in mice with a *S. aureus* infection. Intravenously injected cells are known to become trapped in the lungs 1 h after injection,[44] which is also observed in this study with SPECT after 4 h. This could explain why no signal was detected in the SPECT scans at 4 h. Interestingly, near-infrared fluorescence (NIRF) labeling of cytotoxic T-cells, via biorthogonal conjugation, and in vivo tracking of these cells in tumor-bearing mice have shown that the maximum accumulation time of T-cells was between 2 and 4 days.[46] Although in this study the THP-1 cells were followed for a maximum of 24 h, with 35 000 cells present at the infection site, this was enough to detect a signal with SPECT/CT. However, for future studies, it might be interesting to follow the cells for a longer period of time to study the influx and egress of the THP-1 cells at the infection site. By also monitoring the inflammation progress, one could deduct the effect of the immune cells on the infection progress. Last, labeling the NPs with positron emitters, such as zirconium-89, will enable higher sensitivity imaging with positron emission tomography (PET).

CONCLUSION

Current and future development and implementation of immune cell therapy could benefit from noninvasive in vivo whole-body cell tracking. Therefore, we have developed novel PLGA NPs modified with primary amine groups which enable intrinsic, efficient, stable, and simple ^{111}In-labeling. [^{111}In]In-PLGA-NH_2 NPs can be used for cell labeling and show improved ^{111}In-retention compared with [^{111}In]In-oxine, without affecting on cell viability. Radiolabeled cells can be tracked ex vivo using SPECT/CT and show accumulation in *S. aureus* infection in mice. In conclusion, we have developed a PLGA-NH_2 nanoparticle with favorable characteristics for ex vivo cell radiolabeling. In the future, cell labeling efficiency in specific target cells may be improved by conjugating PLGA-NH_2 NPs with targeting agents such as nanobodies or antibodies. Also, transitioning to PET for higher sensitivity in vivo cell tracking is considered.

MATERIALS AND METHODS

For more detail, see Supporting Information.

Synthesis of Nanoparticles. PLGA-NH_2 NPs were prepared as described previously,[8] with one difference that we used polymers with a primary amine linker.

Characterization of Nanoparticles. All batches of PLGA NPs were analyzed for size, PDI, and zeta potential. For size and PDI, 0.1 mg/mL of NPs was dissolved in Milli-Q while for the zeta potential, the same concentration was dissolved in 5 mM NaCl pH 7.4 and both characteristics were measured with a Zetasizer Nano ZS (Malvern Instruments, Worcestershire, United Kingdom). The results were evaluated with Malvern software (Zetasizer software, Ink) using cumulant fitting. Further characteristics of size and shape of the NPs were obtained from atomic force microscopy (AFM, Catalyst BioScope, Bruker) coupled to a Leica confocal microscope (TCS SP5II). A 100 μL (1 mg/mL) suspension of particles was transferred to and dried on clean glass substrates. Particles were imaged in peak-force tapping mode using silicon nitride cantilevers with nominal spring constants of 0.4 N/m (Bruker). NanoScope analysis software (Bruker) was used to analyze the images. PFCE encapsulation efficiency was measured with a nuclear magnetic resonance (NMR, Bruker Avance III 400 MHz) spectrometer with a broad band fluorine observation (BBFO) probe. Mestrenova 10.0.2 was used for data evaluation.

Fluorescamine Conjugation of PLGA and PLGA-NH_2 NPs for Primary Amine Detection. PLGA and PLGA-NH_2 NPs or ratios were dissolved at concentrations of 1 mg/mL in PBS. Fluorescamine (Sigma-Aldrich, Israel) was dissolved at 9 mg/mL in acetone, and 50 μL was added to the NPs and incubated at 37 °C for 5 min. After incubation, the particles were centrifuged at 20 817*g* for 30 min, the supernatant was

https://doi.org/10.1021/acs.bioconjchem.1c00271
Bioconjugate Chem. 2021, 32, 1802−1811

discarded, and the pellet was resuspended in PBS. Fluorescence (excitation: 390 ± 9 nm, emission: 475 ± 20 nm) was measured in triplicate with a Tecan Infinite M200 PRO (Tecan, Austria) and the software Tecan i-control (Tecan).

DTPA Conjugation of PLGA and PLGA-NH_2 NPs. PLGA or PLGA-NH_2 was incubated with a 10 fold molar excess of isothiocyanatobenzyl-diethylenetriaminepentaacetic acid (ITC-DTPA, Macrocyclics, Plano, TX), relative to the molecular weight of 1 mg polymer weight, in 0.1 M $NaHCO_3$ (pH 9.0) buffer at 37 °C for 1 h. The NPs were washed with Milli-Q at room temperature (RT) by centrifugation at 20 817*g* for 30 min and dissolved in 0.5 M ammonium acetate (NH_4Ac, pH 5.5, metal free).

Stability over Time of Nanoparticles in PBS and Human Serum. The size of PLGA and PLGA-NH_2 NPs was examined over time (0, 1, 2, 4, 6, 24, 48, 72, 168, and 336 h) in PBS and 100% human serum (from human male AB plasma, Sigma-Aldrich, St. Louis, MO). Labeling with nonradioactive indium (2.7 ng indium/mg NP in 0.05 M HCl, pH 1.1−1.4, Merck, St. Louis, MO) was performed with the same conditions as during ^{111}In-labeling (see below). A concentration of 10 mg/mL of PLGA and PLGA-NH_2 NP was prepared and incubated at 37 °C. For each time point, the samples were diluted to a concentration of 0.1 mg/mL. Thereafter, the size of the NPs was measured as explained above.

^{111}In-Labeling of PLGA and PLGA-NH_2 NPs. For intrinsic and chelator-based labeling of the NPs, the same labeling conditions were used. Unless otherwise stated, 1−5 MBq of [^{111}In]$InCl_3$ (Curium Netherlands B.V., The Netherlands) was added to 1 mg of NPs dissolved in 0.5 NH_4Ac. The samples were incubated at RT for 30 min and washed with PBS by centrifuging at 20 817*g* for 30 min. For ITC-DTPA-free ^{111}In-labeling, the NPs were directly dissolved in 0.5 M NH_4Ac.

Instant Thin Layer Chromatography (iTLC). After incubation and after washing, iTLC was performed to determine the labeling efficiency and radiochemical purity. Samples were applied to a silica-gel impregnated strip (Agilent Technologies, Santa Clara, CA). The strip was placed in a 0.1 M sodium citrate running buffer (pH 6.0), and the buffer was allowed to migrate to the top. Subsequently, a film was developed with a phosphorluminescence plate and analyzed using a Typhoon FLA 7000 phosphor imager (GE Healthcare Life Science). The images were analyzed using Aida/1D thin layer chromatography software (GE Healthcare Life Science). Unless otherwise stated, the labeling efficiency was 40−50% and radiochemical purity after centrifugation was >95%.

Radiolabel Retention. [^{111}In]in-PLGA-NH_2 NPs (5−7 MBq/mg, 10 mg/mL) were incubated in PBS or 100% human serum at 37 °C for 2 weeks. At every time point (0, 1, 2, 4, 6, 24, 48, 72, 168, and 336 h), samples were analyzed with iTLC.

EDTA Challenge. [^{111}In]In-PLGA-NH_2 NPs (5−7 MBq/mg, 10 mg/mL) were incubated in a solution of 0.1, 1, 10, and 50 mM EDTA in PBS at 37 °C for 2 weeks. At every time point (0, 1, 2, 4, 6, 24, 48, 72, 168, and 336 h), samples were analyzed with iTLC.

Animal Housing and Experiments. Experiments were performed in accordance with the guidelines set for animal care of the Nijmegen and European Animal Experiments Committee, and the animals were maintained in individually ventilated cages blueline. Nine C57BL/6JRj female mice, age 6−8 weeks and an average weight of 20 ± 0.9 g, were obtained from Janvier Laboratories for biodistribution and blood clearance of [^{111}In]In-PLGA-NH_2 NPs (CCD application 2015-0071). BALB/cAnNRj-Foxn1nu/Foxn1nu mice (12 mice, female, Janvier Laboratories) at age 6−8 weeks and average weight of 23.24 ± 1.36 g were used for the in vivo SPECT/CT imaging of [^{111}In]In-THP-1 cells in Matrigel (CCD application 2018-0011). BALB/CAnN.Cg-Foxn1nu/Crl mice (6 mice, female, Charles River) at age 6−8 weeks and average weight of 19.1 ± 1.01 g were used for the *Staphylococcus aureus* (*S. aureus*) model for in vivo tracking of [^{111}In]In-THP-1 cells experiments (CCD application 2020-0007).

Biodistribution and Blood Clearance of [^{111}In]In-PLGA-NH_2 NPs. All nine mice were slowly injected intravenously (iv) via the tail vein with 400 μL containing 20 mg [^{111}In]In-PLGA-NH_2 NPs (20 MBq) in PBS. Blood and organs were collected and weighed, and radioactivity was measured with a γ-counter (Wizard 2480 automatic gamma counter, PerkinElmer, Waltham, MA). The injected dose per gram (%ID/g) in tissue and blood was calculated based on simultaneous measurements of aliquots from injected fluid. The blood half-life ($t_{1/2}$) was calculated with GraphPad Prism using nonlinear regression with one phase decay, which is computed as $\ln(2)/K$, with K as a rate constant, expressed in reciprocal of the X axis time units.

In Vivo SPECT/CT Imaging. Prior to imaging, inhalation anesthesia of isoflurane in oxygen (33% oxygen +66% air) was administered to mice. For induction, 5% isoflurane was used, while during scanning, 1−2% was maintained. Mice from group 1 (n = 3 mice) underwent SPECT/CT imaging at 1 h, 4 h, 24 h, and day 3, while mice from group 2 (n = 3 mice) were imaged at day 3, 1 week, and 2 weeks after injection. Scans were acquired with U-SPECT II/CT system (MILabs), using the following settings: acquisition 30−60 min, 1.0 mm diameter pinhole mouse high sensitivity collimator tube and CT parameters, 160 μm spatial resolution, 615 μA, and 65 kV. Reconstruction was performed with MILabs software, with an energy window of 154 keV minimal and 188 keV maximal range, 1 iteration, 16 subsets, and a voxel size of 0.4 mm. Maximum-intensity projections were created using Inveon Research Workplace software (version 4.1).

Monocyte-Derived Dendritic Cell (moDC) Generation from Donor Patient-Isolated Monocytes. Monocytes were isolated from peripheral blood mononuclear (PBMC) cells from a healthy donor (A+ (ABC/Rh), buffy coats from Sanquin blood bank, The Netherlands). MoDCs were generated according to standard protocols at the department. For more details, see Supporting Information.

Confocal Imaging of moDC Labeled with Fluorescent PLGA and PLGA-NH_2. MoDC were placed in a 24-well plate (100 000 cells/well) containing coverslips (1/2 Micro Coverglass 12 mm diameter, Electron Microscopy Sciences, Hatfield, PA). The cells were left to adhere overnight at culture conditions. Next, some samples received 0.2 mg of PLGA NPs or PLGA-NH_2 NPs dissolved in PBS, while negative controls received PBS. After incubating the samples for 2 h, the cells were washed with PBS, fixed with 4% paraformaldehyde, stained for membrane with Alexa Flour-488-conjugated wheat germ agglutinin (ThermoFisher, W11261), diluted (1:1000) in carbo free buffer, and incubated in the dark at RT for 10 min. Mounting medium was added before the coverslips were mounted on the microscope slides (Superfrost Plus, Thermo

https://doi.org/10.1021/acs.bioconjchem.1c00271
Bioconjugate Chem. 2021, 32, 1802−1811

Fisher Scientific, Waltham, MA). A Zeiss laser scanning microscope 900 with Airyscan was used to acquire the optical sections and z-stack images. Images were analyzed, and videos were composed with Fiji. In addition, Adobe Photoshop (version 21.0.3) was used to increase the brightness in all images for optimal visualization.

[^{111}In]In-PLGA-NH$_2$ NP and [^{111}In]In-Oxine Labeling of moDC Cells and Radiolabel Retention over Time. NPs were ^{111}In-labeled as described above. This experiment was performed in triplicate. MoDC cells were incubated with [^{111}In]In-PLGA-NH$_2$ NPs (5.52 MBq/mg) in RPMI-1640 at culture conditions for 2 h. In parallel, moDC cells were labeled with [^{111}In]In-oxine (Curium Netherlands B.V., The Netherlands) method for similar specific activity and incubated at RT on a shaker for 15−20 min. After labeling, cells were washed with PBS and resuspended in RPMI-1640 medium and incubated at culture conditions for 1, 2, 4, 6, 24, and 48 h. To determine the retention of the NPs by the moDC cells, the amount cell-associated radioactivity was measured before and after one wash step at every time point. Radiolabel retention was calculated as the fraction still cell associated after washing. Cells were stained with trypan blue and counted with Luna Cell Counting Slides (Logos biosystems, South Korea). The measured activity per sample and the number of cells counted were used to calculate the specific activity per cell or million cells.

Cell Culture. Immortalized human monocyte cell line THP-1 (passage <20, ATCC TIB-202, Manassas, VA) and human adenocarcinoma cell line MDA-MB-231 (passage 46, CL161102_004) were cultured in RPMI-1640 medium (Gibco, Life Technologies Limited, United Kingdom) supplemented with 10% focal bovine serum (FBS, Brazilian origin, Sigma-Aldrich, St. Louis, MO) and 1% L-glutamine (200 mM, Gibco, Life Technologies Limited, United Kingdom) at 37 °C, 5% CO_2 and humid environment.

In Vivo SPECT/CT Imaging of [^{111}In]In-THP-1 Cells in Matrigel. At day 0, mice were subcutaneously (sc) injected with 200 μL of 10 000 (12 ± 13 kBq, n = 4) or 100 000 (70 ± 34 kBq, n = 4) [^{111}In]In-THP-1 cells, or 2.31 ± 1.10 μg [^{111}In]In-PLGA-NH$_2$ NPs (67 ± 31 kBq, n = 4) in PBS mixed with Matrigel (1:1 (v/v) PBS:Matrigel, BD Matrigel matrix basement membrane (20.20 mg/mL), BD Biosciences, United Kingdom) on the right flank. At 1 and 24 h post transplantation, SPECT/CT images were acquired as described previously. After scanning, blood, Matrigel, and organs were harvested and measured ex vivo as described previously.

***S. aureus* Model for in Vivo Tracking of [^{111}In]In-THP-1 Cells.** *S. aureus* were purchased from QM Diagnostics (2.06 × 10^9 colony forming units (CFU)/mL PBS). At day −2, blood was extracted from one donor mouse and mixed (1:1) with the *S. aureus* and 50 μL was directly injected in the right hind leg muscle of five mice. As a control, donor blood was mixed with PBS (1:1) and 50 μL was injected in the contralateral hind leg muscle of the same mice. At day 0, [^{111}In]In-THP-1 cells (5 × 10^6 cells/mouse, 1.30 ± 0.14 MBq/mouse) were injected iv via the tail vein. MicroSPECT/CT imaging and ex vivo biodistribution studies were performed as described previously.

CellTiter-Glo Cell ATP Production Assay. CellTiter-Glo assay was performed according to manufacturer's protocol, and bioluminescence was measured with Tecan Infinite M200 PRO and software Tecan i-control (attenuation automatic, integration time 1000 ms, settle time 0 ms).

Statistical Analysis. GraphPad Prism software was used for statistical analysis. Statistical difference between two groups with a Gaussian distribution was determined with a two-tailed, unpaired, Student's t test; p-values <0.05 are considered statistically significant. For comparisons of three or more groups a one-way ANOVA test with a Tukey test correction of multiple comparisons was performed. In addition, for the organ biodistribution, a two-way ANOVA test with a Sidak test correction of multiple comparisons was performed. All comparisons were based on a minimum of three replicates.

■ ASSOCIATED CONTENT

Supporting Information

The Supporting Information is available free of charge at https://pubs.acs.org/doi/10.1021/acs.bioconjchem.1c00271.

Additional experimental data, biodistribution tables, and a materials and methods section (PDF)

Confocal z-stack video (AVI)

Confocal z-stack video (AVI)

Confocal z-stack video (AVI)

■ AUTHOR INFORMATION

Corresponding Author

Massis Krekorian − *Department of Tumor Immunology, Radboud Institute for Molecular Life Sciences, Radboud University Medical Center, 6525 GA Nijmegen, The Netherlands; Department of Medical Imaging, Radboud Institute for Molecular Life Sciences, Radboud university Medical Center, 6525 GA Nijmegen, The Netherlands;* orcid.org/0000-0002-5812-866X; Email: massis.krekorian@radboudumc.nl

Authors

Gerwin G. W. Sandker − *Department of Medical Imaging, Radboud Institute for Molecular Life Sciences, Radboud university Medical Center, 6525 GA Nijmegen, The Netherlands*

Kimberley R. G. Cortenbach − *Department of Tumor Immunology, Radboud Institute for Molecular Life Sciences, Radboud University Medical Center, 6525 GA Nijmegen, The Netherlands*

Oya Tagit − *Department of Tumor Immunology, Radboud Institute for Molecular Life Sciences, Radboud University Medical Center, 6525 GA Nijmegen, The Netherlands;* orcid.org/0000-0002-5773-6647

N. Koen van Riessen − *Department of Tumor Immunology, Radboud Institute for Molecular Life Sciences, Radboud University Medical Center, 6525 GA Nijmegen, The Netherlands; Cenya Imaging BV, 1052 RK Amsterdam, The Netherlands*

René Raavé − *Department of Medical Imaging, Radboud Institute for Molecular Life Sciences, Radboud university Medical Center, 6525 GA Nijmegen, The Netherlands*

Mangala Srinivas − *Department of Tumor Immunology, Radboud Institute for Molecular Life Sciences, Radboud University Medical Center, 6525 GA Nijmegen, The Netherlands; Cenya Imaging BV, 1052 RK Amsterdam, The Netherlands;* orcid.org/0000-0002-3835-1995

Carl G. Figdor − *Department of Tumor Immunology, Radboud Institute for Molecular Life Sciences, Radboud*

University Medical Center, 6525 GA Nijmegen, The Netherlands

Sandra Heskamp − *Department of Medical Imaging, Radboud Institute for Molecular Life Sciences, Radboud university Medical Center, 6525 GA Nijmegen, The Netherlands;* orcid.org/0000-0001-7250-0846

Erik H. J. G. Aarntzen − *Department of Medical Imaging, Radboud Institute for Molecular Life Sciences, Radboud university Medical Center, 6525 GA Nijmegen, The Netherlands*

Complete contact information is available at: https://pubs.acs.org/10.1021/acs.bioconjchem.1c00271

Notes

The authors declare the following competing financial interest(s): M.S. and NKvR work for Cenya Imaging BV, the Netherlands.

■ ACKNOWLEDGMENTS

We also thank Olga Koshkina, Edyta Swider, Alexander H. J. Staal, Raffaela Rossin, Thuur van Onzen, Peter Laverman, and Mark Rijpkema for their helpful discussions and Gerben Franssen, Milou Boswinkel, and Annemarie Kip for their practical support. We also thank the Microscope Imaging Centre (MIC) at the Radboudumc Institute for Molecular Life Sciences (RIMLS) for letting us use the Zeiss laser scanning microscope 900. M.S. received a European Research Council (ERC) starting grant (CoNQUeST, grant 336454) and grant 14716 from The Netherlands Organisation for Scientific Research NWO-TTW. S.H. is supported by The Netherlands Organisation for Scientific Research (NWO, project number 91617039) and the Dutch Cancer Society (KWF, project number 10099). E.A. received Junior Researcher grants from the Radboud Institute for Molecular Life Sciences (RIMLS) and Dutch Cancer Society Young Investigator Grant (project 12493) and is supported by a grant from the Radboud Oncologie Fonds/Stichting Bergh in het Zadel, partner of Dutch Cancer Society (KUN2015-8106).

■ REFERENCES

(1) Liu, Z., and Li, Z. (2014) Molecular imaging in tracking tumor-specific cytotoxic T lymphocytes (CTLs). *Theranostics 4* (10), 990−1001.

(2) Fruhwirth, G. O., Kneilling, M., de Vries, I. J. M., Weigelin, B., Srinivas, M., and Aarntzen, E. H. J. G. (2018) The Potential of In Vivo Imaging for Optimization of Molecular and Cellular Anti-cancer Immunotherapies. *Mol. Imaging Biol. 20* (5), 696−704.

(3) Roca, M., de Vries, E. F J., Jamar, F., Israel, O., and Signore, A. (2010) Guidelines for the labelling of leucocytes with 111In-oxine. *Eur. J. Nucl. Med. Mol. Imaging 37* (4), 835−841.

(4) de Vries, E. F. J., Roca, M., Jamar, F., Israel, O., and Signore, A. (2010) Guidelines for the labelling of leucocytes with 99mTc-HMPAO. *Eur. J. Nucl. Med. Mol. Imaging 37* (4), 842−848.

(5) Park, J.-J., Lee, T.-S., Son, J.-J., Chun, K.-S., Song, I.-H., Park, Y.-S., Kim, K.-I., Lee, Y.-J., and Kang, J.-H. (2012) Comparison of Cell-Labeling Methods with 124 I-FIAU and 64 Cu-PTSM for Cell Tracking Using Chronic Myelogenous Leukemia Cells Expressing HSV1-tk and Firefly Luciferase. *Cancer Biother. Radiopharm. 27* (10), 719−728.

(6) Makadia, H. K., and Siegel, S. J. (2011) Poly Lactic-co-Glycolic Acid (PLGA) as Biodegradable Controlled Drug Delivery Carrier. *Polymers (Basel, Switz.) 3* (3), 1377−1397.

(7) Kim, K.-T., Lee, J.-Y., Kim, D.-D., Yoon, I.-S., and Cho, H.-J. (2019) Recent Progress in the Development of Poly(lactic-co-glycolic acid)-Based Nanostructures for Cancer Imaging and Therapy. *Pharmaceutics 11* (6), 280.

(8) Srinivas, M., Cruz, L. J., Bonetto, F., Heerschap, A., Figdor, C. G., and de Vries, I. J. M. (2010) Customizable, multi-functional fluorocarbon nanoparticles for quantitative in vivo imaging using 19F MRI and optical imaging. *Biomaterials 31* (27), 7070−7077.

(9) Swider, E., Koshkina, O., Tel, J., Cruz, L. J., de Vries, I. J. M., and Srinivas, M. (2018) Customizing poly(lactic-co-glycolic acid) particles for biomedical applications. *Acta Biomater. 73*, 38−51.

(10) Koshkina, O., Lajoinie, G., Baldelli Bombelli, F., Swider, E., Cruz, L. J., White, P. B., Schweins, R., Dolen, Y., van Dinther, E. A. W., van Riessen, N. K., et al. (2019) Multicore Liquid Perfluorocarbon-Loaded Multimodal Nanoparticles for Stable Ultrasound and 19 F MRI Applied to In Vivo Cell Tracking. *Adv. Funct. Mater. 1806485*, 1806485.

(11) Swider, E., Daoudi, K., Staal, A. H. J., Koshkina, O., van Riessen, N. K., van Dinther, E., de Vries, I. J. M., de Korte, C. L., and Srinivas, M. (2018) Clinically-applicable perfluorocarbon-loaded nanoparticles for in vivo photoacoustic, ^{19}F magnetic resonance and fluorescent imaging. *Nanotheranostics. 2* (3), 258−268.

(12) Krekorian, M., Fruhwirth, G. O., Srinivas, M., Figdor, C. G., Heskamp, S., Witney, T. H., and Aarntzen, E. H. J. G. (2019) Imaging of T-cells and their responses during anti-cancer immunotherapy. *Theranostics 9* (25), 7924−7947.

(13) Udenfriend, S., Stein, S., Böhlen, P., Dairman, W., Leimgruber, W., and Weigele, M. (1972) Fluorescamine: A reagent for assay of amino acids peptides proteins and primary amines in the picomole range. *Science (Washington, DC, U. S.) 178* (4063), 871−872.

(14) Staal, A. H. J., Becker, K., Tagit, O., van Riessen, N. K., Koshkina, O., Veltien, A., Bouvain, P., Cortenbach, K. R. G., Scheenen, T., Flögel, U., et al. (2020) NC-ND license. *Biomaterials 261*, 120307.

(15) Wongrakpanich, A., Morris, A. S., Geary, S. M., Joiner, M. A., and Salem, A. K. (2017) Surface-modified particles loaded with CaMKII inhibitor protect cardiac cells against mitochondrial injury. *Int. J. Pharm. 520* (1−2), 275−283.

(16) Walkey, C. D., Olsen, J. B., Guo, H., Emili, A., and Chan, W. C. W. (2012) Nanoparticle size and surface chemistry determine serum protein adsorption and macrophage uptake. *J. Am. Chem. Soc. 134* (4), 2139−2147.

(17) Walkey, C. D., Olsen, J. B., Song, F., Liu, R., Guo, H., Olsen, D. W. H., Cohen, Y., Emili, A., and Chan, W. C. W. (2014) Protein corona fingerprinting predicts the cellular interaction of gold and silver nanoparticles. *ACS Nano 8* (3), 2439−2455.

(18) Nel, A. E., Mädler, L., Velegol, D., Xia, T., Hoek, EM V., Somasundaran, P., Klaessig, F., Castranova, V., and Thompson, M. (2009) Understanding biophysicochemical interactions at the nano-bio interface. *Nat. Mater. 8* (7), 543−557.

(19) Jiang, W., von Roemeling, C. A., Chen, Y., Qie, Y., Liu, X., Chen, J., and Kim, B. Y. S. (2017) Designing nanomedicine for immuno-oncology. *Nat. Biomed Eng. 1* (2), 0029.

(20) Tabata, Y., and Ikada, Y. (1988) Macrophage phagocytosis of biodegradable microspheres composed of L-lactic acid/glycolic acid homo-and copolymers. *J. Biomed. Mater. Res. 22* (10), 837−858.

(21) Maxwell, G. R. Synthetic nitrogen products. *Handbook of Industrial Chemistry and Biotechnology*, 12th ed.; Springer, 2012; p 875.

(22) Shaffer, T. M., Wall, M. A., Harmsen, S., Longo, V. A., Drain, C. M., Kircher, M. F., and Grimm, J. (2015) Silica nanoparticles as substrates for chelator-free labeling of oxophilic radioisotopes. *Nano Lett. 15* (2), 864−868.

(23) Good, N. E., Winget, G. D., Winter, W., Connolly, T. N., Izawa, S., and Singh, R. M. Hydrogen Ion Buffers for Biological Research. *Biochemistry* 1966, *5*, 467−477.

(24) Kandegedara, A., and Rorabacher, D. B. (1999) Non-complexing tertiary amines as "better" buffers covering the range of pH 3−11. Temperature dependence of their acid dissociation constants. *Anal. Chem. 71* (15), 3140−3144.

(25) Panagi, Z., Beletsi, A., Evangelatos, G., Livaniou, E., Ithakissios, D. S., and Avgoustakis, K. (2001) Effect of dose on the biodistribution and pharmacokinetics of PLGA and PLGA-mPEG nanoparticles. *Int. J. Pharm. 221* (1−2), 143−152.
(26) Qie, Y., Yuan, H., von Roemeling, C. A., Chen, Y., Liu, X., Shih, K. D., Knight, J. A., Tun, H. W., Wharen, R. E., Jiang, W., et al. (2016) Surface modification of nanoparticles enables selective evasion of phagocytic clearance by distinct macrophage phenotypes. *Sci. Rep. 6* (1), 1−11.
(27) Wang, H., Wu, L., and Reinhard, B. M. (2012) Scavenger receptor mediated endocytosis of silver nanoparticles into J774A.1 macrophages is heterogeneous. *ACS Nano 6* (8), 7122−7132.
(28) Tsoi, K. M., Macparland, S. A., Ma, X. Z., Spetzler, V. N., Echeverri, J., Ouyang, B., Fadel, S. M., Sykes, E. A., Goldaracena, N., Kaths, J. M., et al. (2016) Mechanism of hard-nanomaterial clearance by the liver. *Nat. Mater. 15* (11), 1212−1221.
(29) De Jong, W. H., Hagens, W. I., Krystek, P., Burger, M. C., Sips, A.J. A. M., and Geertsma, R. E. (2008) Particle size-dependent organ distribution of gold nanoparticles after intravenous administration. *Biomaterials 29* (12), 1912−1919.
(30) Xiao, K., Li, Y., Luo, J., Lee, J. S., Xiao, W., Gonik, A. M., Agarwal, R. G., and Lam, K. S. (2011) The effect of surface charge on in vivo biodistribution of PEG-oligocholic acid based micellar nanoparticles. *Biomaterials 32* (13), 3435−3446.
(31) Cataldi, M., Vigliotti, C., Mosca, T., Cammarota, M., and Capone, D. (2017) Emerging Role of the Spleen in the Pharmacokinetics of Monoclonal Antibodies, Nanoparticles and Exosomes. *Int. J. Mol. Sci. 18* (6), 1249.
(32) Swider, E., Staal, A. H. J., van Riessen, N. K., Jacobs, L., White, P. B., Fokkink, R., Janssen, G.-J., van Dinther, E., Figdor, C. G., de Vries, I. J. M., et al. (2018) Design of triphasic poly(lactic-*co* -glycolic acid) nanoparticles containing a perfluorocarbon phase for biomedical applications. *RSC Adv. 8* (12), 6460−6470.
(33) Kassis, A. I., and Adelstein, S. J. Chemotoxicity of indium-111 oxine in mammalian cells. *J. Nucl. Med.* 1985, *26* (2), 187−190.
(34) Gildehaus, F. J., Haasters, F., Drosse, I., Wagner, E., Zach, C., Mutschler, W., Cumming, P., Bartenstein, P., and Schieker, M. (2011) Impact of indium-111 oxine labelling on viability of human mesenchymal stem cells in vitro and 3D cell-tracking using SPECT/CT in vivo. *Mol. Imaging Biol. 13* (6), 1204−1214.
(35) Malviya, G., Nayak, T., Gerdes, C., Dierckx, R. A. J. O., Signore, A., and de Vries, E. F. J. (2016) Isolation and 111In-Oxine Labeling of Murine NK Cells for Assessment of Cell Trafficking in Orthotopic Lung Tumor Model. *Mol. Pharmaceutics 13* (4), 1329−1338.
(36) Fernández-Barahona, I., Muñoz-Hernando, M., Pellico, J., Ruiz-Cabello, J., and Herranz, F. (2018) Molecular Imaging with 68Ga Radio-Nanomaterials: Shedding Light on Nanoparticles. *Appl. Sci. 8* (7), 1098.
(37) Khan, I., Gothwal, A., Kaul, A., Mathur, R., Mishra, A. K., and Gupta, U. (2018) Radiolabeled PLGA Nanoparticles for Effective Targeting of Bendamustine in Tumor Bearing Mice. *Pharm. Res. 35* (11), 1−11.
(38) Snehalatha, M., Venugopal, K., Saha, R. N., Babbar, A. K., and Sharma, R. K. (2008) Etoposide Loaded PLGA and PCL Nanoparticles II: Biodistribution and Pharmacokinetics after Radiolabeling with Tc-99m. *Drug Delivery 15* (5), 277−287.
(39) Llop, J., Jiang, P., Marradi, M., Gómez-Vallejo, V., Echeverrí, M., Yu, S., Puigivila, M., Baz, Z., Szczupak, B., Pé, R.-C. C, et al. (2015) Visualisation of dual radiolabelled poly(lactide-co-glycolide) nanoparticle degradation in vivo using energy-discriminant SPECT. *J. Mater. Chem. B 3*, 6293.
(40) Tang, J., Baxter, S., Menon, A., Alaarg, A., Sanchez-Gaytan, B. L., Fay, F., Zhao, Y., Ouimet, M., Braza, M. S., Longo, V. A., et al. (2016) Immune cell screening of a nanoparticle library improves atherosclerosis therapy. *Proc. Natl. Acad. Sci. U. S. A. 113* (44), E6731−E6740.
(41) Sirianni, R. W., Zheng, M. Q., Patel, T. R., Shafbauer, T., Zhou, J., Saltzman, W. M., Carson, R. E., and Huang, Y. (2014) Radiolabeling of poly(lactic-co-glycolic acid) (PLGA) nanoparticles with biotinylated F-18 prosthetic groups and imaging of their delivery to the brain with positron emission tomography. *Bioconjugate Chem. 25* (12), 2157−2165.
(42) Keliher, E. J., Yoo, J., Nahrendorf, M., Lewis, J. S., Marinelli, B., Newton, A., Pittet, M. J., and Weissleder, R. (2011) 89Zr-labeled dextran nanoparticles allow in vivo macrophage imaging. *Bioconjugate Chem. 22* (12), 2383−2389.
(43) Trujillo-Nolasco, R. M., Morales-Avila, E., Ocampo-García, B. E., Ferro-Flores, G., Gibbens-Bandala, B. V., Escudero-Castellanos, A., and Isaac-Olive, K. (2019) Preparation and in vitro evaluation of radiolabeled HA-PLGA nanoparticles as novel MTX delivery system for local treatment of rheumatoid arthritis. *Mater. Sci. Eng., C 103*, 109766.
(44) Bonios, M., Terrovitis, J., Chang, C. Y., Engles, J. M., Higuchi, T., Lautamäki, R., Yu, J., Fox, J., Pomper, M., Wahl, R. L., et al. (2011) Myocardial substrate and route of administration determine acute cardiac retention and lung biodistribution of cardiosphere-derived cells. *J. Nucl. Cardiol. 18* (3), 443−450.
(45) Chandrasekaran, R., Madheswaran, T., Tharmalingam, N., Bose, R. J., Park, H., and Ha, D. H. (2021) Labeling and tracking cells with gold nanoparticles. *Drug Discovery Today 26* (1), 94−105.
(46) Kim, W., Yoon, H. Y., Lim, S., Stayton, P. S., Kim, I. S., Kim, K., and Kwon, I. C. (2021) In vivo tracking of bioorthogonally labeled T-cells for predicting therapeutic efficacy of adoptive T-cell therapy. *J. Controlled Release 329*, 223−236.
(47) Harmsen, S., Medine, E. I., Moroz, M., Nurili, F., Lobo, J., Dong, Y., Turkekul, M., Pillarsetty, N. V. K., Ting, R., Ponomarev, V., et al. (2021) A dual-modal PET/near infrared fluorescent nanotag for long-term immune cell tracking. *Biomaterials 269*, 120630.
(48) Sehl, O. C., Gevaert, J. J., Melo, K. P., Knier, N. N., and Foster, P. J. (2020) A Perspective on Cell Tracking with Magnetic Particle Imaging. *Tomography. 6* (4), 315−324.

https://doi.org/10.1021/acs.bioconjchem.1c00271
Bioconjugate Chem. 2021, 32, 1802−1811